Supporting Information for

Carbazole-based Polysiloxane Hosts for Highly Efficient Solution-processed Blue Electrophosphorescent Devices

Dianming Sun, Qiang Fu, Zhongjie Ren,* Wei Li, Huihui Li, Dongge Ma, and Shouke Yan*

Experimental Section

General Information:

^{1}H NMR and ^{13}C NMR spectra were measured on a Bruker AV400 (400MHz) spectrometer. Chemical shifts (δ) are given in parts per million (ppm) relative to tetramethylsilane (TMS; $\delta=0$) as the internal reference. ^{1}H NMR spectra data are reported as chemical shift, relative integral, multiplicity (s=singlet, d=doublet, m=multiplet), coupling constant (J in Hz) and assignment.

Elemental analyses of carbon, hydrogen, and nitrogen were performed on a Vario EL cube.

UV-Vis absorption spectra were recorded on a Shimadzu UV-3600 recording spectrophotometer.

PL spectra were recorded on a Hitachi F-7000 fluorescence spectrophotometer. Differential scanning calorimetry (DSC) was performed on a TA Q2000 Differential Scanning Calorimeter at a heating rate of 10 ^{o}C min^{-1} from 25 to 200 ^{o}C under nitrogen atmosphere. The glass transition temperature (T_g) was determined from the second heating scan.

Thermogravimetric analysis (TGA) was undertaken with a METTLER TOLEDO TGA/DSC 1/1100SF instrument. The thermal stability of the samples under a nitrogen atmosphere was determined by measuring their weight loss while heating at a rate of 10 ^{o}C min^{-1} from 25 to 800 ^{o}C.

AFM images were obtained on a Agilent-5500 AFM in the tapping mode.

Cyclic voltammetry (CV) was carried out in nitrogen-purged dichloromethane (oxidation scan) at room temperature with a CHI voltammetric analyzer. Tetrabutylammonium hexafluorophosphate (TBAPF$_6$) (0.1M) was used as the supporting electrolyte. The conventional three-electrode configuration consists of a glassy carbon working electrode, a platinum wire auxiliary electrode, and an Ag/AgCl pseudo-reference electrode with ferrocenium–ferrocene (Fc$^+$/Fc) as the internal standard. Cyclic voltammograms were obtained at scan rate of 100 mV s^{-1}. The onset potential was determined from the intersection of two tangents drawn at the rising and background current of the cyclic voltammogram

Nanoindentation Methodology on thin films: Nanoindentation was performed at ambient

temperature using an MTS NanoIndenter® XP (MTS Corp., Eden Prairie, MN), equipped with the Continuous Stiffness Measurement (CSM) module. A three sided pyramidal Berkovich tip (tip radius ~100 nm) was used to determine the Young's modulus (E) and hardness (H). The indenter axes were aligned normal to the as prepared thin films. The loading part of both facets is smooth, indicating that the plastic deformation, which occurs underneath the Berkovich tip during indentation, is relatively homogeneous in nature. The average values of elastic modulus (E) and hardness (H) of sample, extracted from the P-h curves, are calculated over depths of 100 – 1,000 nm in order to minimize the imperfection of the Berkovich tip.[1] The Young's modulus (E) and hardness (H) are calculated as a function of surface penetration depth (h) using the dynamic CSM mode. This is accomplished by continuously monitoring the change of the elastic contact stiffness (S) determined from the P-h curves, then the reduced modulus (E_r)[2] was extracted:

$$E_r = \frac{\sqrt{\pi}}{2\beta} \frac{S}{\sqrt{A_c}}$$

where A_c is the contact area under load (based on the calibrated tip area function) and β is a constant that depends on the geometry of the indenter ($\beta = 1.034$ for a Berkovich tip). The method proposed by Oliver and Pharr ($O\&P$)[3] was used to extract the sample elastic modulus from the reduced modulus assumes isotropic elastic properties, as described in the following equation:

$$\frac{1}{E_r} = \frac{1-v_i^2}{E_i} + \frac{1-v_s^2}{E_s}$$

Where v and E are Poisson's ratio and elastic modulus, respectively; and the subscripts i and s refer to the indenter and test material, respectively. The indenter properties used in this study are $E_i = 1141$ GPa, and Poisson's ratio for the indenter is $v_i = 0.07$. In the main article, the elastic modulus from the thin film was calculated using $v_s = 0.3$.

The hardness of a material is defined as its resistance to local plastic deformation. Thus, indentation hardness, H, can be determined from the maximum indentation load, P_{max}, divided by the contact area, A_c[3-4]:

$$H = \frac{P_{max}}{A_c}$$

Where the contact area (A_c) is a function of the contact depth, hc, and can be determined by the following equation:

$$A_c(h_c) = C_0 h_c^2 + C_1 h_c + C_2 h_c^{1/2} + C_3 h_c^{1/4} + \ldots\ldots + C_8 h_c^{1/128}$$

It may be noted that only the constant C_0 is used, if it is assumed that a Berkovich indenter has a perfect tip. However, for imperfect tips, higher-order terms have to be taken into account and these are obtained from the tip-area function curve fit for a given tip.

The contact depth can be estimated from the load-displacement data using

$$h_c = h_{max} - \varepsilon \frac{P_{max}}{S}$$

where h_{max} is the maximum indentation depth and 0.75(P/S) denotes the extent of elastic recovery (h_e).

References:

1. Gong, J.; Miao, H.; Peng, Z. *Mater. Lett.* **2004**, *58*, 1349.

2. (a) Oliver, W. C.; Pharr, G. M. *J. Mater. Res.* **1992**, *7*, 1564; (b) Oliver, W. C.; Pharr, G. M. *J. Mat. Res.* **2004**, *19*, 3.

3. (a) Vlassak, J. J.; Nix, W. D. *J. Mech. Phys. Solids* **1994**, *42*, 1223; (b) Bei, H.; George, E. P.; Pharr, G. M. *Scripta Materialia* **2004**, *51*, 875; (c) Cripps, A. C. F. *Introduction to Contact Mechanics*, Second Edition, Springer, New South Wales, Australia, **2007**.
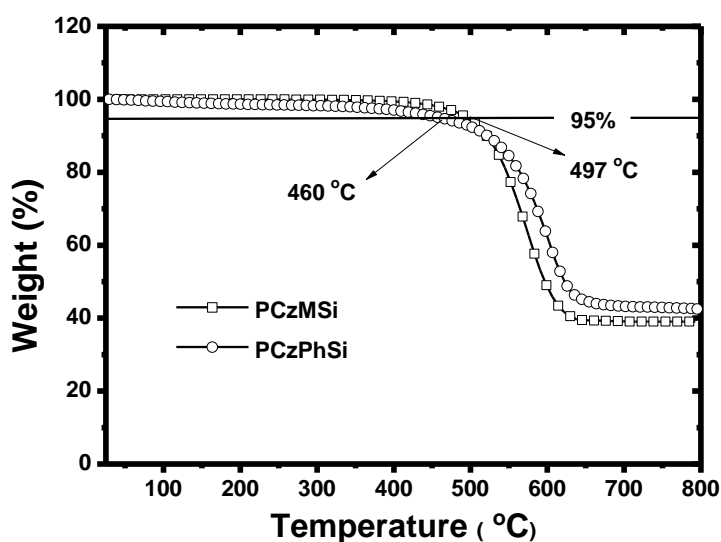
Figure S1. TGA thermograms of PCzMSi and PCzPhSi recorded at a heating rate of 10 °C min^{-1}.
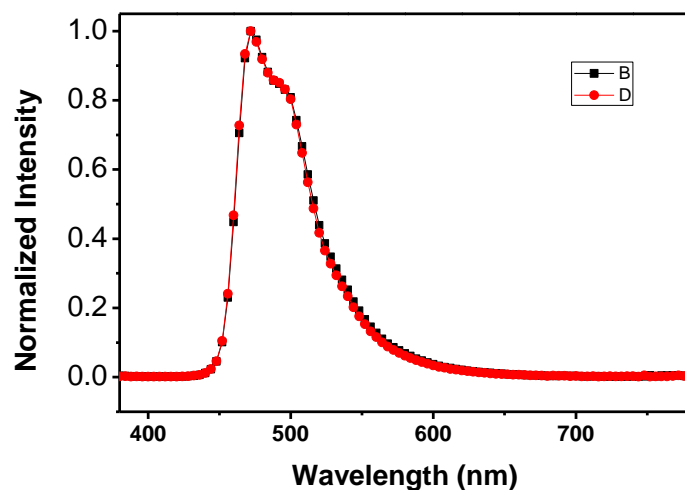
Figure S2. a) Device structures [ITO/ PEDOT:PSS (40 nm)/ Host (PCzMSi and PCzPhSi): 10 wt% FIrpic (40-45 nm)/ Tm3PyPB (5 nm)/ TPBI (30 nm)/ LiF (1 nm)/Al (100nm)] and the corresponding energy level diagram. b) Normalized EL spectra of blue PhOLED at 100 cd m^{-2}.
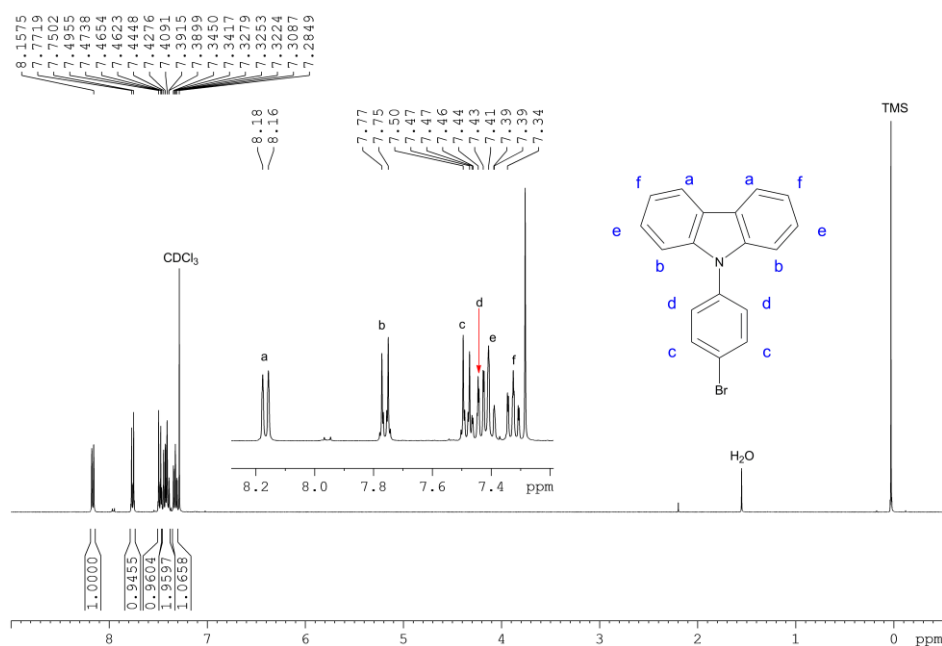

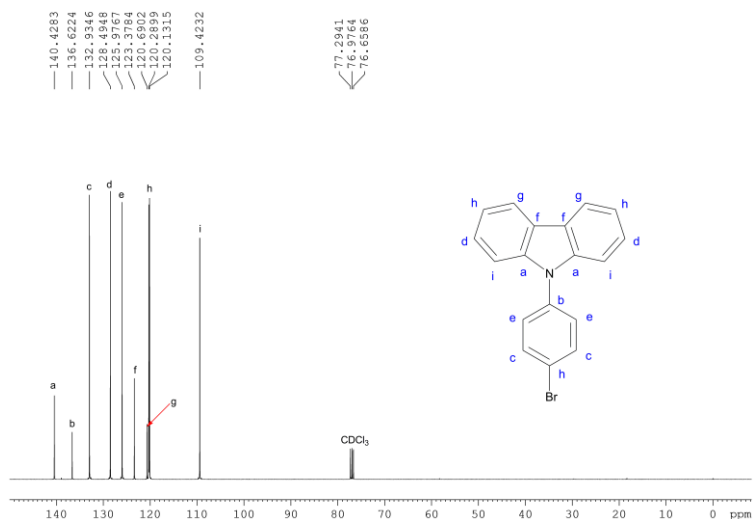**Figure S3.** ^{1}H NMR spectrum of 9-(4-bromophenyl)-9-carbazole.

Figure S4. ^{13}C NMR spectrum of 9-(4-bromophenyl)-9-carbazole.
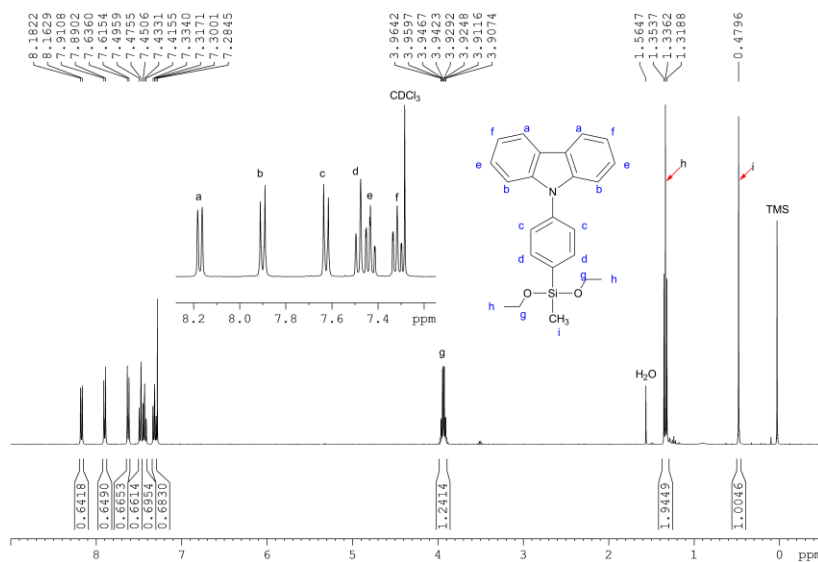
Figure S5. ^{1}H NMR spectrum of 9-(4-(diethoxy(methyl)silyl)phenyl)-9-carbazole.
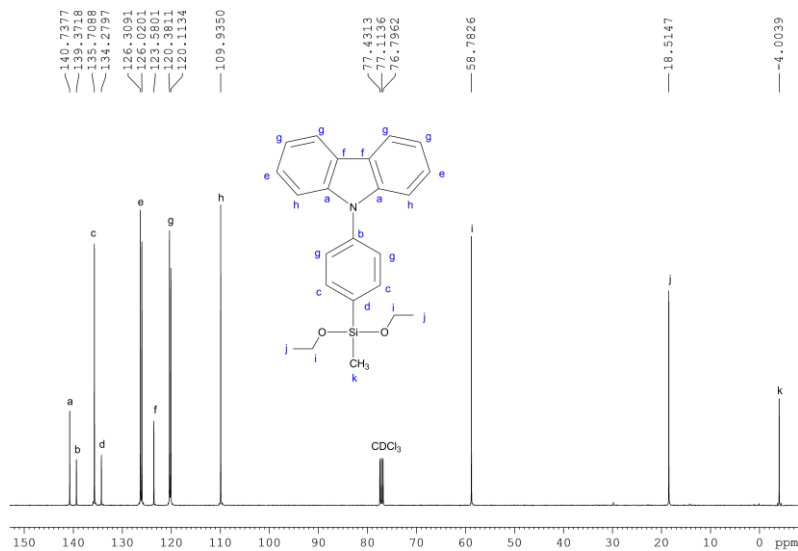
Figure S6. ^{13}C NMR spectrum of 9-(4-(diethoxy(methyl)silyl)phenyl)-9-carbazole.
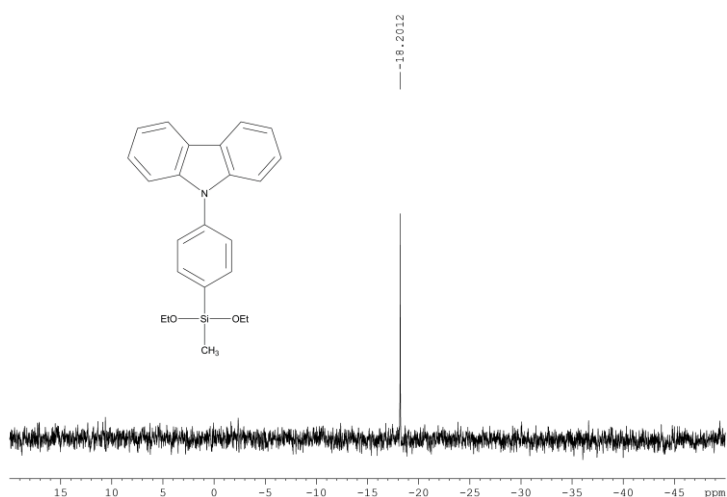
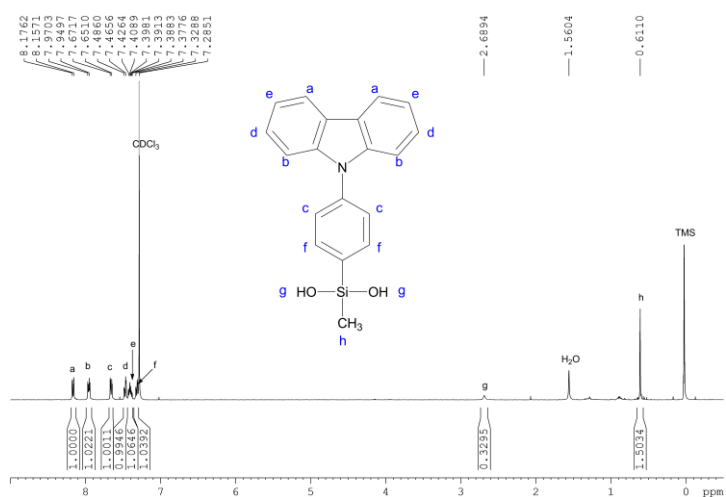**Figure S7.** ^{29}Si NMR spectrum of 9-(4-(diethoxy(methyl)silyl)phenyl)-9-carbazole.

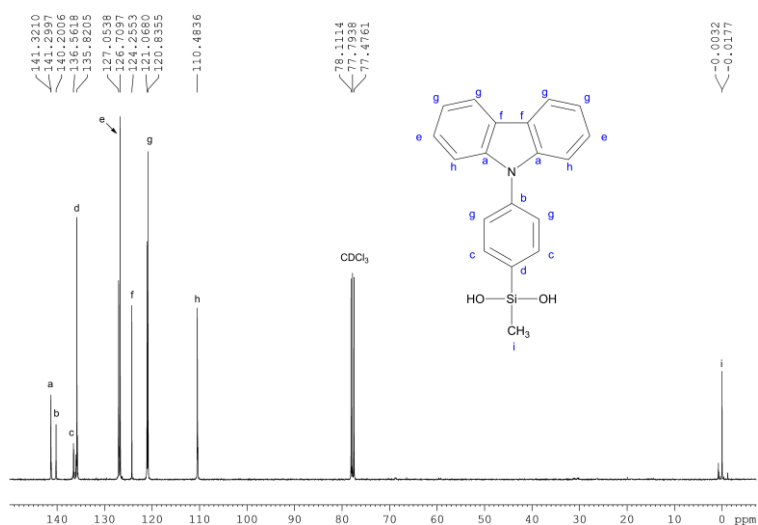**Figure S8.** ^{1}H NMR spectrum of (4-(9-carbazol-9-yl)phenyl)(methyl)silanediol.

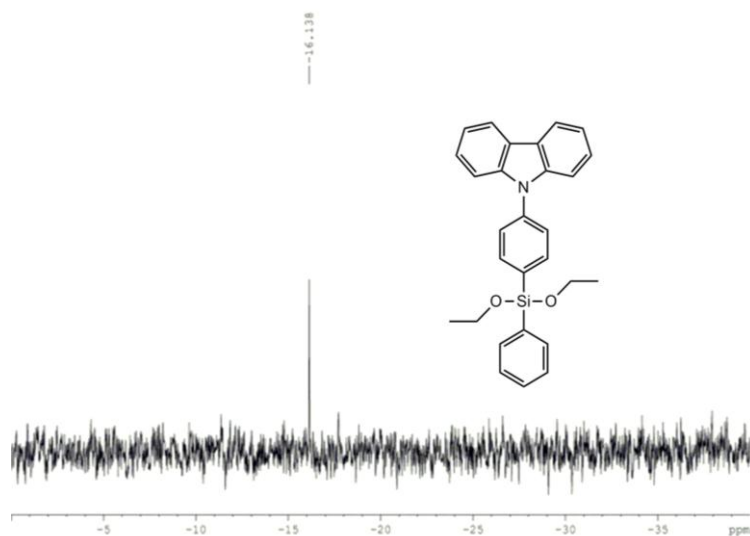**Figure S9.** ^{13}C NMR spectrum of (4-(9-carbazol-9-yl)phenyl)(methyl)silanediol.

Figure S10. ^{29}Si NMR spectrum of (4-(9-carbazol-9-yl)phenyl)(methyl)silanediol.

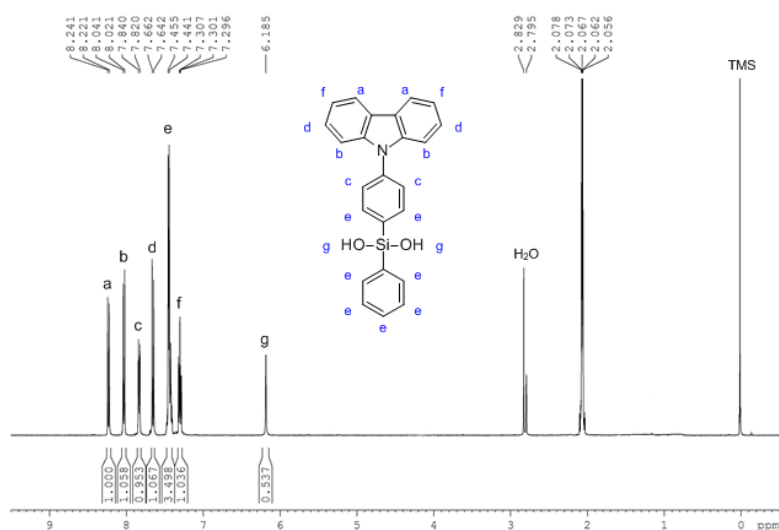**Figure S11.** ^{1}H NMR spectrum of 9-(4-(diethoxy(phenyl)silyl)phenyl)-9-carbazole

Figure S12. ^{13}C NMR spectrum of 9-(4-(diethoxy(phenyl)silyl)phenyl)-9-carbazole

Figure S13. ^{29}Si NMR spectrum of 9-(4-(diethoxy(phenyl)silyl)phenyl)-9-carbazole

Figure S14. ^{1}H NMR spectrum of (4-(9H-carbazol-9-yl)phenyl)(phenyl)silanediol
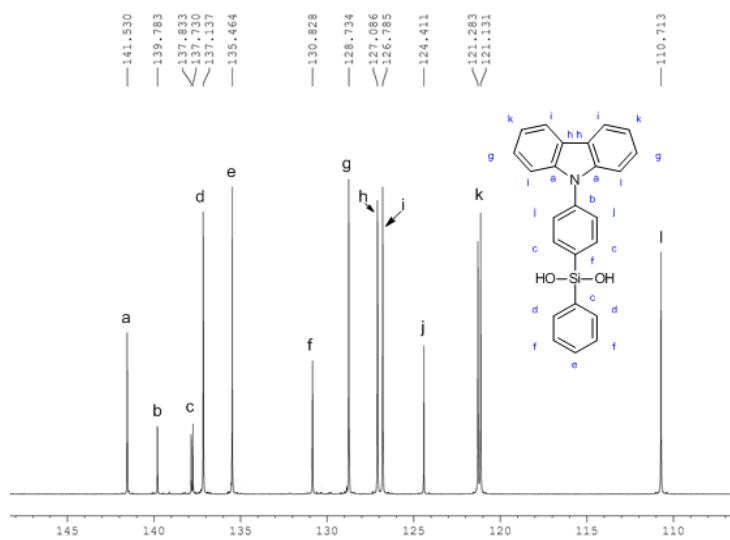

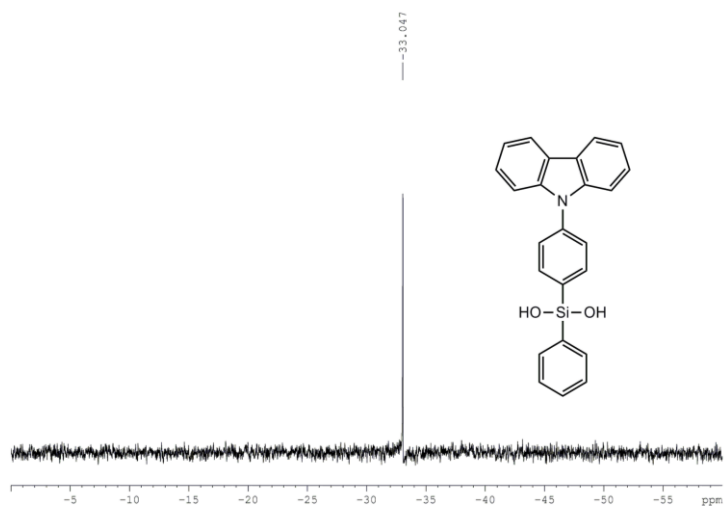**Figure S15.** ^{13}C NMR spectrum of (4-(9H-carbazol-9-yl)phenyl)(phenyl)silanediol

8

Figure S16. ^{29}Si NMR spectrum of (4-(9H-carbazol-9-yl)phenyl)(phenyl)silanediol
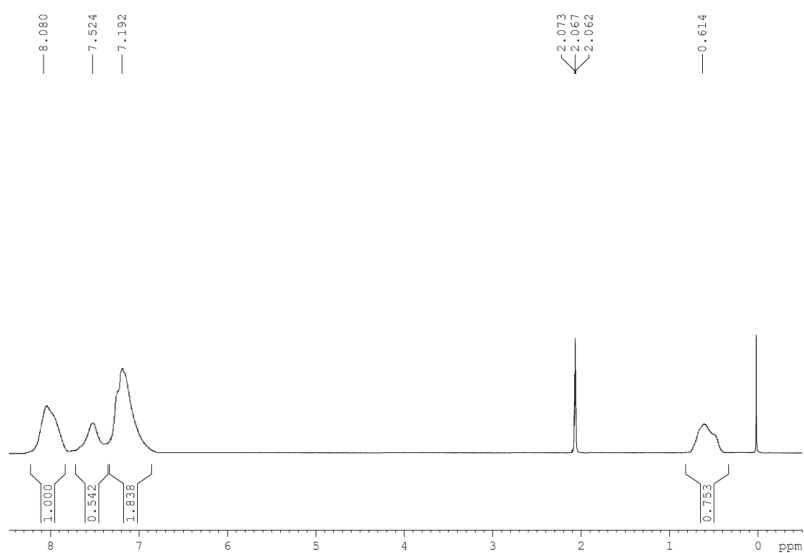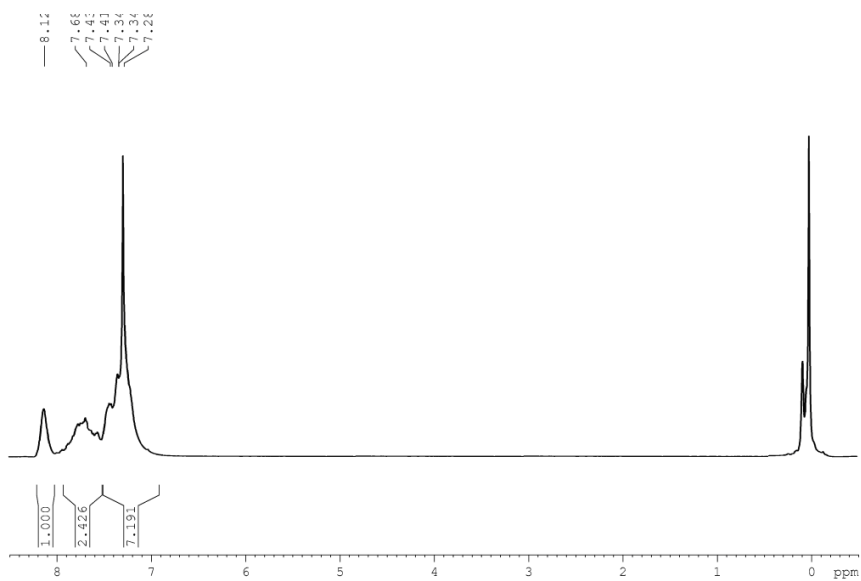

Figure S17. ^{1}H NMR spectrum of **PCzMSi**

9

Figure S18. ^{1}H NMR spectrum of **PCzPhSi**